EDUCACIÓN
SECRETARÍA DE EDUCACIÓN PÚBLICA

Instituto Politécnico Nacional
"La Técnica al Servicio de la Patria"

Research in Computing Science

Vol. 155 No. 1
January 2026

Research in Computing Science

Research in Computing Science, Año 25, Volumen 155, No. 1, enero de 2026, es una publicación mensual, editada por el Instituto Politécnico Nacional, a través del Centro de Investigación en Computación. Av. Juan de Dios Bátiz S/N, Esq. Av. Miguel Othon de Mendizábal, Col. Nueva Industrial Vallejo, C.P. 07738, Ciudad de México, Tel. 57 29 60 00, ext. 56571. https://www.rcs.cic.ipn.mx. Editor responsable: Dr. Grigori Sidorov. Reserva de Derechos al Uso Exclusivo del Título No. 04-2019-082310242100-203. ISSN: en trámite, ambos otorgados por el Instituto Politécnico Nacional de Derecho de Autor. Responsable de la última actualización de este número: el Centro de Investigación en Computación, Dr. Grigori Sidorov, Av. Juan de Dios Bátiz S/N, Esq. Av. Miguel Othon de Mendizábal, Col. Nueva Industrial Vallejo, C.P. 07738. Fecha de última modificación 01 de enero de 2026.

Research in Computing Science, year 25, Volume 155, No. 1, January 2026, is published monthly by the Center for Computing Research of IPN.

Volume 155(1)

Advances in Optics and Photonics

Blanca Cecilia López-Ramírez (ed.)

Instituto Politécnico Nacional, Centro de Investigación en Computación
México 2026

ISSN: in process

Formerly ISSNs: 1870-4069, 1665-9899

Instituto Politécnico Nacional (IPN)
Centro de Investigación en Computación (CIC)
Av. Juan de Dios Bátiz s/n esq. M. Othón de Mendizábal
Unidad Profesional "Adolfo López Mateos", Zacatenco
07738, México D.F., México

http://www.rcs.cic.ipn.mx
http://www.ipn.mx
http://www.cic.ipn.mx

Indexed in LATINDEX, DBLP and Periodica

Electronic edition

ISSN 1870-4069

Table of Contents

Page

ISSN 1870-4069

Characterization of Temperature-induced Changes in Polarization-maintaining Nonlinear Optical Fibers

Miguel A. Espiricueta-Ulloa[1,*], Javier Sánchez-Mondragón[2], Julio C. García-Melgarejo[1], Néstor Lozano-Crisóstomo[1]

[1] Universidad Autónoma de Coahuila, Facultad de Ingeniería Mecánica y Eléctrica, Mexico

[2] Instituto Nacional de Astrofísica, Óptica y Electrónica, Puebla, Mexico

arturo_espiricueta@uadec.edu.mx

Abstract. We theoretically characterize the temperature-induced changes in polarization-maintaining (PM) nonlinear optical fibers. Based on a linear model of the temperature-dependent birefringence, we compute the change of the output polarization state (PS) of light through the calculation of the Stokes parameters. Our treatment provides an important analysis for the implementation in nonlinear temperature sensors.

Keywords: Polarization-maintaining nonlinear optical fibers, temperature-dependent birefringence, nonlinear polarization conversion, optical fiber sensors.

1 Introduction

The theory for describing and controlling the nonlinear polarization conversion of circularly polarized (CP) light in nonlinear birefringent optical fibers (BOFs) (Low- and High-BOFs) is given in [4]. Through a nonlinear model, it was provided the conditions to obtain the most common continuous wave (CW) polarization states (PSs) at the BOF output. In that regard, all-optical nonlinear control of CP light was demonstrated by tailoring the nonlinear and birefringence fiber parameters. Such results are very important because open new perspectives for all-optical fiber sensors and provide considerable physical insight on the all-optical polarization control with nonlinear BOFs.

In this work, we characterize the temperature-induced changes in PM nonlinear optical fibers through the computing of the change of the output PS of light. For this purpose, we develop a theoretical model to show how the birefringence is affected by the temperature changes.

2 Temperature Sensing Mechanism

We begin by considering a CW CP light beam launched into a lossless PM fiber such that it excites the two orthogonally polarized modes. The coupled-mode equations that describe the evolution of the two orthogonally polarized components are given by [1]:

$$\frac{\mathrm{d}U_x}{\mathrm{d}z} = i\frac{1}{L_{NL}}\left(|U_x|^2 + \frac{2}{3}|U_y|^2\right)U_x + i\frac{1}{3L_{NL}}U_x^* U_y^2 \mathrm{e}^{-i2\Delta\beta z}, \tag{1a}$$

$$\frac{\mathrm{d}U_y}{\mathrm{d}z} = i\frac{1}{L_{NL}}\left(|U_y|^2 + \frac{2}{3}|U_x|^2)\right)U_y + i\frac{1}{3L_{NL}}U_y^* U_x^2 \mathrm{e}^{+i2\Delta\beta z}. \tag{1b}$$

Here $U_x(z)$ and $U_y(z)$ are the normalized slowly varying amplitudes of such orthogonal polarization components of the optical field. Here the factor $i = \sqrt{-1}$ represents the imaginary unit, z is the standard notation for the propagation distance, $L_{NL} = (\gamma P_0)^{-1}$ is the nonlinear length, P_0 is the input peak power, and γ is the nonlinear parameter. The linear birefringence parameter is $\Delta\beta = 2\pi/L_B$, where $L_B = \lambda/B$ is the beat length, $B = |n_x - n_y|$ is the degree of modal birefringence, and λ is the wavelength of light. n_x and n_y are the effective refractive indices along the x- and y-polarization axes of the PM fiber, respectively. It is usually assumed that n_x along the x-polarization or slow axis is greater than n_y along the y-polarization or fast axis.

Solutions of Eqs. (1a) and (1b) can be given by the following matrix form representation which describes the evolution of the two normalized slowly varying amplitudes, $U_x(z)$ and $U_y(z)$, along a PM fiber [4]

$$\begin{bmatrix} U_x(z) \\ U_y(z) \end{bmatrix} = \mathbf{M}(z) \begin{bmatrix} U_x(0) \\ U_y(0) \end{bmatrix}. \tag{2}$$

Here $U_x(0)$ and $U_y(0)$ represent the normalized slowly varying amplitudes of the two orthogonally polarized modes of the input signal field. The propagation matrix $\mathbf{M}(z)$ given by:

$$\mathbf{M}(z) = \begin{bmatrix} t\mathrm{e}^{i(\phi_{NL\pm} - \Delta\beta z/2)} & \pm ir\mathrm{e}^{i(\phi_{NL\mp} - \Delta\beta z/2)} \\ \pm ir\mathrm{e}^{i(\phi_{NL\mp} + \Delta\beta z/2)} & t\mathrm{e}^{i(\phi_{NL\pm} + \Delta\beta z/2)} \end{bmatrix}, \tag{3}$$

is satisfied when either right hand circular polarization (RHCP) or left hand circular polarization (LHCP) light is launched into the PM fiber. Here $\phi_{NL+}(z)$ and $\phi_{NL-}(z)$ are two nonlinear phase shifts, and $t(z) = \sqrt{1+u(z)}/\sqrt{2}$ and $r(z) = i\sqrt{1-u(z)}/\sqrt{2}$ are defined as the transmittance and reflectance, respectively. In general, before relations satisfy the conservation of energy conditions: $|t(z)|^2 + |r(z)|^2 = 1$ and $r(z)t^*(z) + t(z)r^*(z) = 0$. In Eq. (3), the upper and lower signs in $\pm$ and $\mp$ are considered to be associated with the RHCP and LHCP input light, respectively.

The $u(z)$, $\phi_{NL+}(z)$ and $\phi_{NL-}(z)$ functions are given by

$$u = \mathrm{cn}(\Delta\beta z|m), \tag{4a}$$

$$\phi_{NL+}(z) = \frac{5}{6}z \mp \frac{1}{2}\arccos[\mathrm{dn}(\Delta\beta z|m)], \tag{4b}$$

$$\phi_{NL-}(z) = \frac{5}{6}z \pm \frac{1}{2}\arccos[\mathrm{dn}(\Delta\beta z|m)]. \tag{4c}$$

Where $\mathrm{cn}(x|m)$ and $\mathrm{dn}(x|m)$ are two Jacobi elliptic functions with argument x and modulus $m = k^2$. For any elliptic function, its modulus must lie between 0 and 1. In our case, the modulus $m = [\gamma P_0/(3\Delta\beta)]^2$; and therefore, $k = \gamma P_0/(3\Delta\beta)$.

2.1 Methodological Strategy

Power variations of the propagating light and physical parameters, such as temperature, stress, magnetic field, and torsion affect the birefringence of an optical fiber. Thereby some analytical models that relate such physical parameters with the birefringence of optical fibers have been developed [2,3,5]. In that regard, such intuitive relations can be used to implement such theoretical model [4] and develop high-sensitivity all-optical fiber sensors and new sensing methods that allow obtaining magnitudes of parameters more accurately. For our purposes, we implement the following approach given by [2,5]

$$B = B_0 + \gamma_b(T + T_0), \tag{5}$$

where T is the temperature of the fiber under test, T_0 is the room temperature, B_0 is the birefringence at room temperature, and γ_b is the thermal coefficient, which relates the birefringence with temperature in High-BOFs. Therefore, we can use such relation and introduce it in the developed theoretical model through the definition of the beat length given by $l_B = \lambda/B$. In this way, we can apply the theoretical model to analyze how the temperature affects the output polarization in optical fibers. For this purpose, the change of the output PS of initially CW CP light must be monitored after its transmission through a PM fiber.

3 Results

Using Eq. (5), it is possible to calculate the birefringence changes of the High-BOF due to the temperature increments or decrements. Therefore, applying the theory given in [4] and using Eq. (5), we obtain theoretically how the temperature changes affect the Stokes parameters of the output polarized light.

4 Conclusions

We have described and characterized theoretically the temperature-induced changes in PM nonlinear optical fibers through the computing of the change of the

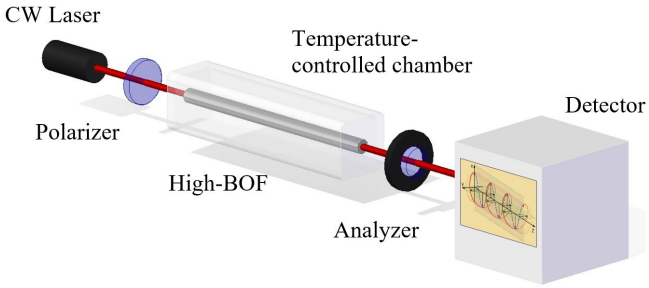

Fig. 1. A light beam traveling through a High-BOF (polarization-maintaining fiber) affected by a specific temperature, changing its physical proprieties and the polarization of light.

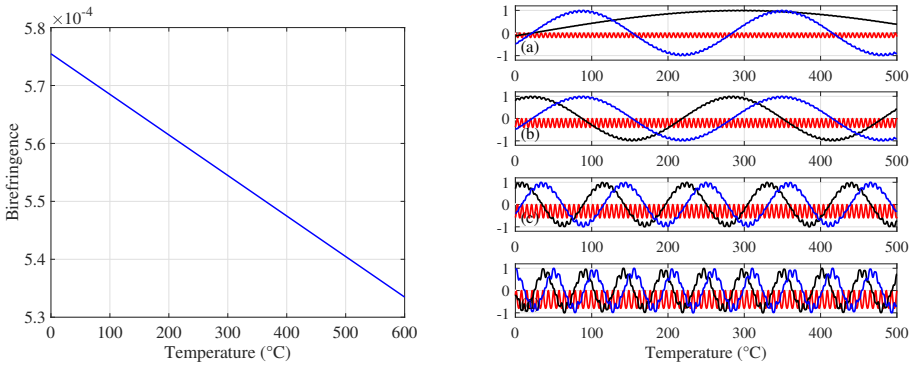

Fig. 2. The graph on the left shows the behavior of fiber's birefringence with increasing temperature, and the graph on the right shows how the Stokes parameters change as the temperature increases. S_1 (red solid line), S_2 (black solid line,) and S_3 (blue solid line). Output Stokes parameters for a High-BOF length $L = 2\ m$, $\lambda = 1550\ nm$, $\gamma_b = -7x10^{-8}\ °C^{-1}$, $T_0 = 20\ °C$, and $B_0 = 5.74x10^{-4}$ [3,5]. Normalized input power for (a) $P_0/P_c = 0.2$, (b) $P_0/P_c = 0.4$, (c) $P_0/P_c = 0.6$ and (d) $P_0/P_c = 0.8$,when a right-handed circularly polarized light is launched into the PM fiber.

output PS of light. We have developed a theoretical model to show how the birefringence is affected by the temperature changes. Our study creates a new possible way to measure temperature utilizing this kind of fibers that we know they are a good option because of their properties.

Acknowledgments. M. A. Espiricueta-Ulloa, N. Lozano-Crisóstomo and J. C. García-Melgarejo thank to the UAdeC for its amazing support.

References

1. Agrawal, G.P.: Nonlinear Fiber Optics. Academic Press, 5 edn. (2013)

2. Ding, Z., Meng, Z., Yao, X.S., Chen, X., Liu, T., , Qin, M.: Accurate method for measuring the thermal coefficient of group birefringence of polarization-maintaining fibers (2011)
3. Kim, D.H., Kang, J.U.: Analysis of temperature-dependent birefringence of a polarization-maintaining photonic crystal fiber (2007)
4. Lozano-Crisóstomo, N., García-Melgarejo, J.C., González-Galicia, M.A., Baez-López, C.A., Hurtado-Carrazco, J.C., Sánchez-Mondragón, J.J.: All-optical nonlinear control of circularly polarized light in birefringent fiber (2021)
5. Thorlabs (2021), designer and manufacturer of photonics equipment for research "https://www.thorlabs.com/newgrouppage9.cfm?objectgroup_id=14214"

ISSN 1870-4069

Band Structures of a Photonic Crystal Waveguide with Koch Snowflake Fractal Structures

Eduardo Mellado Villaseñor[1], Hugo Alva Medrano[2], Héctor Pérez Aguilar[1]

[1] Universidad Michoacana de San Nicolás de Hidalgo,
Facultad de Ciencias Físico Matemáticas,
Mexico

[2] Instituto Tecnológico de Morelia,
Departamento de Ciencias Básicas,
Mexico

hiperezag@yahoo.com

Abstract. Many applications used today are based on the study of certain geometric tools; for example, a peculiar geometry known as fractals. In this work an integral method was developed to calculate the band structures of a photonic crystal waveguide, formed by two parallel conducting plates and an array of inclusions involving Koch snowflake fractal structures. The numerical technique is known as the Integral Equation Method, which starts from Green's second identity to solve the two-dimensional Helmholtz equation. We found that varying the inclusion size for several iterations of the Koch fractal structure allows us to control the band structure of the system. The results show the appearance of several band gaps that substantially modify the photonic band structure. Furthermore, it is possible to obtain discrete modes for a certain frequency range and then the periodic photonic crystal waveguide acts as an unimodal filter. These optical properties exhibit some interest from a technological point of view.

Keywords: Photonic band structures, Koch snowflake, band gaps, integral equation method.

1 Introduction

By analyzing certain geometric tools with the aim of being used in many research methods, this leads to the discovery of applications of great interest [1]. For example, a very peculiar geometry known as fractals, these appear both in nature and in the exact sciences [2]. Scattering of light by fractal surfaces has attracted some attention over the years, with the research reported so far being based on approximate approaches to the scattering equations or with reentrant fractals [3]. On the other hand, the determination of the band structure, reflectance, and

transmittance of one- and two-dimensional photonic crystals with a complex unit cell structure, such as fractal geometries, has been developed based on the solution of integral equations [4]. In this context, we present a theoretical and numerical study of the electromagnetic response of a photonic crystal waveguide (PCW) based on the adoption Koch snowflake fractal structures. To solve this problem, it was done using a numerical technique known as the Integral Equation Method (IEM) [4, 5], which starts from Green's second identity to solve the two-dimensional Helmholtz equation. This paper is organized as follows. In Sec. 2 we introduce an integral method for calculating the dispersion relation to determine the band structures of PCW with Koch snowflake fractal structures, based on ideas described in [4, 5]. Sec. 3 shows the numerial results of band structures of the considered system for different inclusion sizes with several iterations of the Koch fractal structures. Finally, Sec. 4 presents our conclusions.

2 Theoretical Approach

We consider a two-dimensional PCW, formed by two flat internal walls that enclose an array of Koch snowflake fractal structures. The surfaces involved are perfectly-conductive materials and the medium between the walls and the inclusions is vacuum. The geometry of the system is sketched in Fig. 1. In PCW we consider a period P in the flat profiles, a separation between the plates of the waveguide plates given by b and the Koch fractal inclusions for a given iteration, which can be in terms of the side length L of the original triangle.

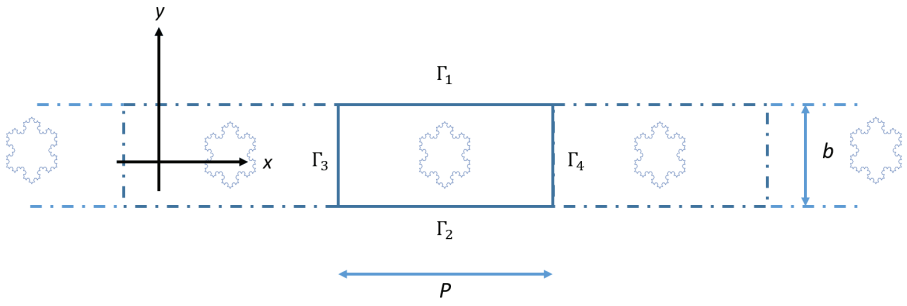

Fig. 1. Schematic description of a periodic waveguide with inclusions formed with perfectly-conductive Koch fractal structures.

2.1 Integral Equation Method

Assuming a time dependency $e^{-i\omega t}$ for electromagnetic fields, the wave equation can be transformed into the Helmholtz equation:

$$\nabla^2 \Psi_j(\mathbf{r}) + n_j^2(\omega)\frac{\omega^2}{c^2}\Psi_j(\mathbf{r}) = 0, \tag{1}$$

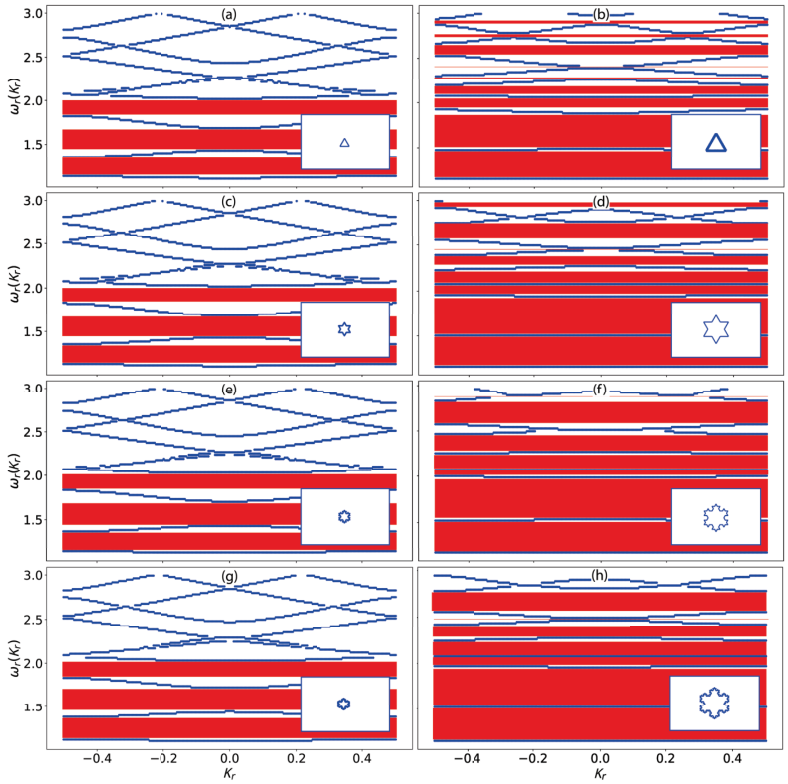

Fig. 2. Photonic band structures of the perfectly conducting PCW that is formed with an array of Koch fractal inclusions of (a) and (b) 0, (c) and (d) 1, (e) and (f) 2, (g) and (h) 3 iterations for the side lengths $L = 1/3$ (first column) and $L = 1$ (second column) of the original triangle. The band gaps are represented by the red stripes. The insets on the right show unit cells in real space whose cross sections of inclusions are made up of Koch snowflake fractals of various orders.

where j indicates the j-th medium with refractive index $n_j = \sqrt{\varepsilon_j}$ forming the system under study begin ε_j the electric permittivity, which is shown in Fig. 1. In Eq. (1) ω is the frequency of the electromagnetic wave, c is the speed of light in vacuum, and $\mathbf{r} = x\hat{\mathbf{i}} + y\hat{\mathbf{j}}$ is independent of z. The function Ψ^j represents the electric or magnetic field and the polarization TE is considered in this work. To solve Eq. (1), we introduce a Green function $G(\mathbf{r}, \mathbf{r}')$, as the solution of the equation given by:

$$\nabla^2 G_j(\mathbf{r}, \mathbf{r}') + n_j^2(\omega)\frac{\omega^2}{c^2} G_j(\mathbf{r}, \mathbf{r}') = -4\pi\delta(\mathbf{r} - \mathbf{r}'), \tag{2}$$

where $\delta(\mathbf{r}-\mathbf{r}')$ is the Dirac delta. A Green function that is a solution of Eq. (2) is given by:

$$G_j(\mathbf{r},\mathbf{r}') = i\pi H_0^1 n_j \left(\frac{\omega|\mathbf{r}-\mathbf{r}'|}{c}\right), \tag{3}$$

with $H_0^1(z)$ the Hankel function of the first kind and zero order.

Applying Green's second integral theorem [4, 5] for the functions Ψ and G in each region corresponding to the j-th medium:

$$\Psi_j(\mathbf{r})\theta_j(\mathbf{r}) = \frac{1}{4\pi}\int_{\Gamma_j}\left[G_j(\mathbf{r},\mathbf{r}')\frac{\partial\Psi_j(\mathbf{r}')}{\partial n'} - \Psi_j(\mathbf{r}')\frac{G_j(\mathbf{r},\mathbf{r}')}{\partial n'}\right]ds', \tag{4}$$

where $\theta_j(r)$ is a step function whose values is one for all points in the medium j-th and zero otherwise. In Eq. (4) the surface is bounded by the corresponding closed boundary Γ_j and the normal derivative $\partial/\partial n'$ goes outside the boundary Γ_j. To solve Eq. (4) it is necessary to convert the integro-differential equations into matrix equations by means of a rectangle approximation to evaluate the integrals in small intervals. Under this consideration, Eq. (4) is transformed into the system of linear equations where matrix elements L^j_{mn} and N^j_{mn} [4]. The property of periodicity that the system has in the x-direction direction is a condition of symmetry that is especially considered. Due to this property and the form of Eq. (1), Bloch's theorem establishes a periodicity condition as $\Psi(x-P,y) = \Psi(x,y)\mathrm{e}^{-iKP}$ with K the Bloch vector. On the other hand, we have that the boundary conditions along the contours Γ_j are given by $\Psi_n^{(j)} = \Psi_n^{(j+1)} = 0$ and $\partial\Psi_n^{(j)}/\partial n = \partial\Psi_n^{(j+1)}/\partial n$, for TE polarization, where $j = 1$ y 2. With these considerations we find a matrix equations $M(\omega)F(\omega) = 0$, which has a representative matrix M and F the source vector, and both depend on the frequency ω and the Bloch vector K. To determine the frequency ω we define the determinant function:

$$D(K,\omega) = \ln|\det(K,\omega)|, \tag{5}$$

which numerically presents local minimum points that will give us the numerical dispersion relation, $\omega = \omega(K)$.

3 Photonic Band Structures

In this work we are going to introduce dimensionless values, so our results are expressed in terms of the reduced Bloch vector given by $K_r = (P/2\pi)K$ and the reduced frequency $\omega_r = (P/2\pi)\omega$. The photonic band structures of a PCW with an array of perfectly conducting inclusions involving Koch snowflake fractal structures (see Fig. 1) are shown below. The geometrical values of the waveguide taken into account were: $b = \pi\mu$ m and $P = 2\pi\mu$ m.

Figure 2 shows the band structures of the rectangular lattice with Koch snowflake fractals of $n = 0, 1, 2$ and 3 iterations for the side lengths $L = 1/3$ [Figs. 2(a), (c), (e) and (g)] and $L = 1$ [Figs. 2(b), (d), (f) and (h)] of the

original triangle, respectively. The results show the appearance of several band gaps (red stripes) as the size of the inclusions and the order of fractal iterations increases, which substantially modify the photonic band structure. Furthermore, it is possible to obtain discrete modes [Figs. 2(d), (f) and (h)] for a given frequency range and then the PCW with Koch fractal structures can act as a unimodal filter.

4 Conclusions

We applied an integral numerical method to calculate the photonic band structures of a PCW formed by two perfectly conducting parallel plates and an array of of inclusions involving Koch snowflake fractal structures. The numerical results obtained show good accuracy and efficiency of the numerical method applied. In addition, it was found that varying the inclusion size for several iterations of the Koch snowflake fractal allows to control the band structure of the system to some extent. The results show the appearance of several band gaps that substantially modify the photonic band structure. Moreover, it is possible to obtain discrete modes for a certain range of frequencies and then the PCW acts as an unimodal filter. This system is considered as a photonic crystal whose band structures correspond in many respects as a conventional photonic crystal, but using only one material. Therefore, the results of the optical response of a periodic PCW with Koch fractal structures promise excellent and interesting optical applications such as filtering and coding of optical signals.

References

1. Fisher, Y.: Fractal image compression. Fractals, **2**(3), 347–361 (1994)
2. Mandelbrot, B.B.: The fractal geometry of nature. W.H. Freeman, New York (1983)
3. Mendoza-Suárez, A., Méndez, E.R.: Light scattering by a reentrant fractal surface. Applied Optics, **36**(15), 3521–3531 (1997). DOI: 10.1364/AO.36.003521
4. Mendoza-Suárez, A., Villa-Villa, F., Gaspar-Armenta, J.A.: Numerical method based on the solution of integral equations for the calculation of the band structure and reflectance of one- and two-dimensional photonic crystals. Journal of the Optical Society of America B, **23**, 2249–2256 (2006). DOI: 10.1364/JOSAB.23.002249
5. Mendoza-Suárez, A., Pérez-Aguilar, H.: Numerical integral methods to study plasmonic modes in a photonic crystal waveguide with circular inclusions that involve a metamaterial. Photonic Nanostructures, **21**, 1–12 (2016)

ISSN 1870-4069

Spatio-Spectro-Temporal Characterization of Ultrashort Vortex Pulses

Erick R. Baca-Montero, Oleksiy V. Shulika

University of Guanajuato,
Department of Electronics Engineering,
Mexico

er.bacamontero@ugto.mx, oshulika@ugto.mx

Abstract. Due to the promising features of optical vortices a variety of methods have been developed for their generation, however, these methods are mostly intended for CW vortex beams and thus can be hardly usable for generation of ultrashort vortex pulses. A spiral phase plate (SPP) is a robust method for vortex generation with potential to be used in ultrafast optics, however, the resulting vortex is not a pure vortex mode but contains contributions of different radial orders. As well, the SPP exhibits a wavelength-dependent phase shift, due to its material dispersion. Here we present a (3+1)D numerical analysis of the spatio-spectro-temporal properties of ultrashort vortex pulses generated with spiral phase plates characterizing the effects of material dispersion and propagation geometry. These results can serve as a basis for the design of new passive and active devices for singular optics and photonics.

Keywords: Spatio-spectro-temporal characterization, ultrashort vortex pulses.

1 Introduction

Ultrashort vortex pulses are electromagnetic radiation with durations in the order of picoseconds or less (broadband optical spectrum) and that present points where the intensity of the wave is zero around the axis of the beam and the phase is undefined [1].

In recent years the study of vortex pulses has peaked due to their promising features in super-resolution microscopy [7], optical tweezers[6], ultra-fast optical communications[3], quantum computing[9] and astrophysics[4].

Laguerre-Gaussian (LG) modes are the most commonly studied set of vortices. They are derived by solving the paraxial Helmholtz equation in cylindrical coordinates [1].

An LG pulse is given by:

$$u_{p,l}^{LG}(r,\phi,z,t) = \underbrace{\frac{C_{lp}^{LG}}{w(z)}\left(\frac{r\sqrt{2}}{w(z)}\right)^{|l|} L_p^{|l|}\left(\frac{2r^2}{w^2(z)}\right) e^{-\frac{r^2}{w^2(z)}} e^{\frac{-ikr^2}{2\left(z^2+z_R^2\right)}} e^{-il\phi} e^{(i(2p+l+1)\psi)}}_{\text{Laguerre Gaussian Mode Factor}} \underbrace{e^{\frac{-(t-t_0)}{\tau^2}} e^{i\omega_t t}}_{\text{Temporal Profile factor}} \quad (1)$$

Here w_0 is the beam radius at the beam waist, r is the radial distance from the center axis of the beam, z_R is the Rayleigh range, ψ is the Gouy phase, $R(z)$ is the radius of curvature, C_{lp}^{LG} is a normalization constant[1], $L_p^{|l|}$ is the generalized Laguerre polynomial of order p and l, and $w(z)$ is the radius of the beam at a given position z, l is called topological charge and it defines the azimuthal distribution (the amplitude has azimuthal angular dependence, $e^{-il\phi}$) that can be positive or negative indicating left or right circulation, while p defines the radial distribution index. In the temporal factor τ is the duration of the pulse, t_0 is the pulse center time and ω_t is the central angular frequency.

A LG mode retains its intensity profile upon propagation, although with a different width and the Gouy phase changes by multiples $(2p + |l| + 1)\pi/2$ as it travels. For $l = 0$, $p = 0$, the expression eq. 1 reduces to that of an ordinary Gaussian beam, as $L_p^{|l|} = 1$.

Since l is an integer, the phase of the field can only increase or decrease by multiples of 2π as one follows a closed path around the axis of the beam. The radial distribution p gives a number of dark rings nested in the beam profile.

Figure 1 shows a three-dimensional reconstruction of the vortex pulse $LG_{0,1}$ with a duration $\tau = 5fs$ The characteristic zero intensity point at the vortex axis can be observed in figures 1 (a) and (c) which show the spatio-temporal intensity profile $|u(x,y,t)|^2$ and slices through the center of the beam, respectively.

The spiraling nature can be observed in figures 1 (b) and (d) which show isosurfaces of the real part of the complex field, $\Re|u(x,y,t)|$ and of the phase (Here the color scale shows the spatio-temporal intensity profile of the vortex pulse along spiraling phase).

2 Ultrashort OVs Spatio-spectro-temporal Characterization during Propagation and Generation with a Spiral Phase Plate

In this work, the propagation and generation of ultrashort vortex pulses is analyzed using control parameters calculated at the input and output of the model domain, these are the real field value of the electric field, the electric field intensity, the spatially resolved spectral intensity and OI_I the overlap integral

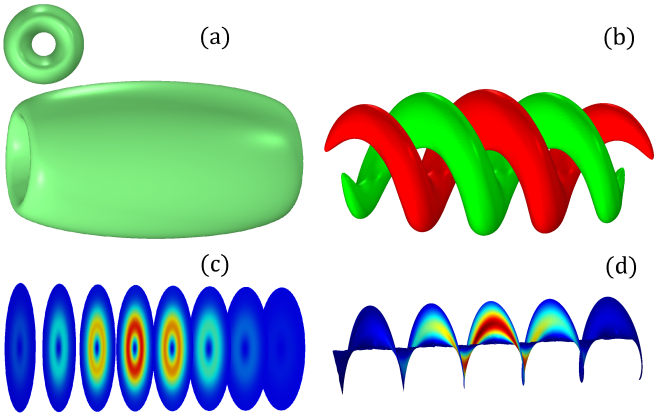

Fig. 1: 3D vortex pulse $LG_{0,1}$ with a duration $\tau = 5fs$: (a) Spatio-temporal intensity profile isosurface set at half of the peak intensity. (b) Isosurfaces of the real part of the complex field. (c) Slices of the characteristic doughnut spatial intensity profile of the vortex pulse along. (d) Isosurface of the spiraling phase of the vortex pulse.

between the amplitude of the analytic LG01 mode (eq. 1) and its numerical counterpart (u_{num}). The overlap integral is given as:

$$OI_I = \frac{\left|\int u_{0,1}^{LG*} u_{num} dA\right|^2}{\int \left|u_{0,1}^{LG}\right|^2 dA \int |u_{num}|^2 dA}, \tag{2}$$

and it gives the quality of vortex modes[2].

2.1 Propagation of ultrashort vortex pulses in dispersive media

The characteristics of a $5fs$ vortex pulse of wavelength $\lambda = 800nm$ upon propagation in a dispersive SiO_2 block of thickness $t = 2\lambda$ are studied. The refractive index of the SiO_2 is given in [5]. Fig. 2 (a) and (b) show the real field amplitude and the overlap integrals (eq. 2) of the vortex before and after propagation, small temporal chirp is acquired (less than $1fs$), while the spatial spectral intensity measured along a line at the left side maximum of the vortex 2 (c) and (d) before and after propagation respectively, shows that the spectrum half amplitude remains constant and therefore the vortex does not present spatial chirp, furthermore, it is then possible to compensate for the time chirp through normal dispersion compensation techniques, as also shown in [8].

2.2 Ultrashort Vortex Generation With a Spiral Phase Plate

A Spiral Phase Plate (SPP) [2] is an optical component for the generation of vortex beams. In this device with refractive index n the optical thickness t is

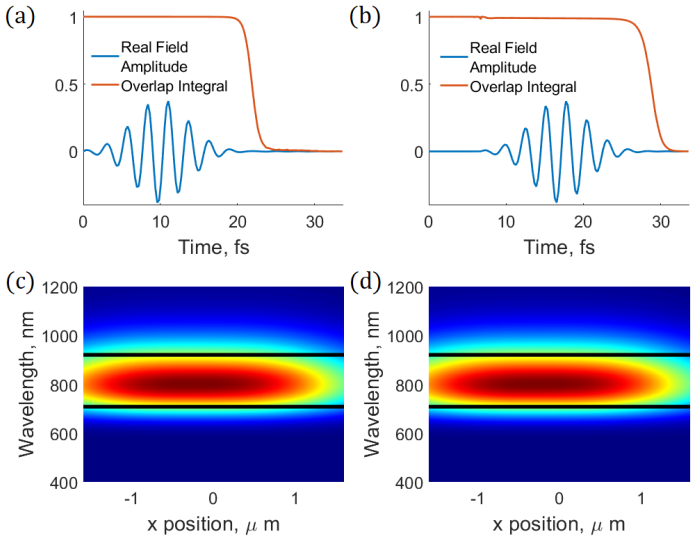

Fig. 2: Spatio-spectro-temporal properties of a vortex pulse upon dispersive propagation in 2λ long SiO_2 block: (a) Real field amplitude of the input vortex pulse and overlap integral (b) Real field amplitude of the vortex pulse and overlap integral after propagation (c) Spatially resolved spectral intensity of the input vortex pulse. (d) Spatially resolved spectral intensity of the output vortex pulse.

varied with an azimuthal angle ϕ according to:

$$t = \phi l \lambda / 2\pi (n - n_b), \tag{3}$$

where λ is the incident beam wavelength and n_b is the refractive index of the medium containing the SPP.

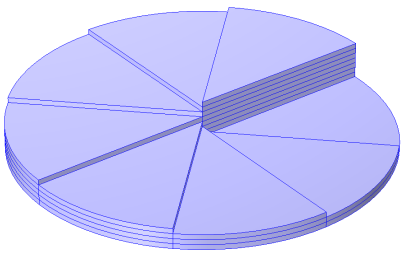

Fig. 3: Schematic of a 8-levels discrete SPP.

Fig. 4 shows the spatio-spectro-temporal properties of the vortex pulse generated with an 8-levels SPP (fig. 3), the spectrum half amplitude (fig. 3 (c) and

(d)) remains constant for the input gaussian pulse and the generated vortex pulse, thus there is no spatial chirp.

The SPP has maximum conversion efficiency (Overlap integral, eq. 2) of 0.73 (fig. 5 (a)), while it presents a conversion efficiency of more than 0.68 in the bandwidth of the pulse (from $700nm$ to $930nm$) (fig. 5 (b)).

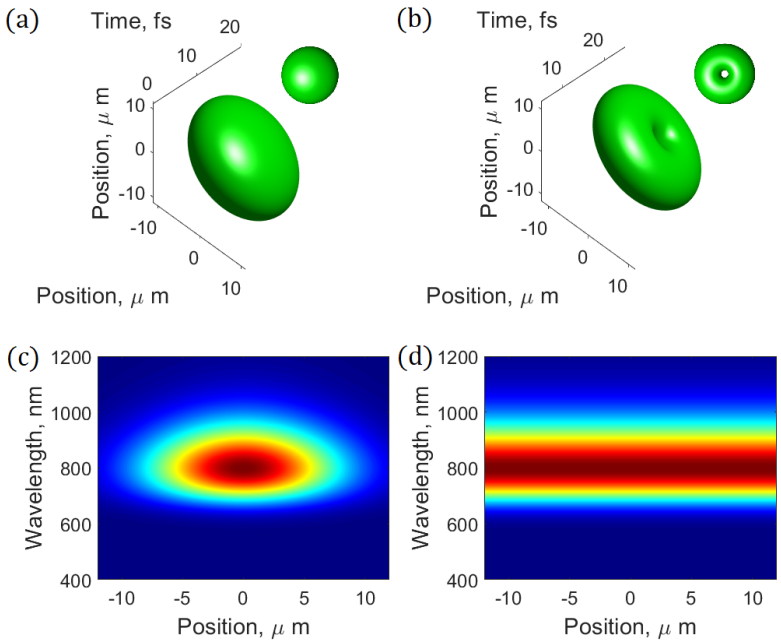

Fig. 4: Spatio-spectro-temporal properties of input pulse to a SPP and of the generated vortex pulse: (a) Spatio-temporal intensity profile isosurface set at half of the peak intensity of the input gaussian pulse. (b) Spatio-temporal intensity profile isosurface set at half of the peak intensity of the generated vortex pulse. (c) Spatially resolved spectral intensity of the input gaussian pulse. (d) Spatially resolved spectral intensity of the generated vortex pulse.

3 Conclusions

In this work, vortex pulses propagation and generation was simulated solving a time-domain wave-equation.

Chromatic dispersion induces temporal broadening of the vortex pulses, while the spatial profile and spatio-spectral properties remain unchanged.

Thus, conventional dispersion compensation techniques can be used to compress back broadened vortices. As well the effect of a SPP chromatic dispersion

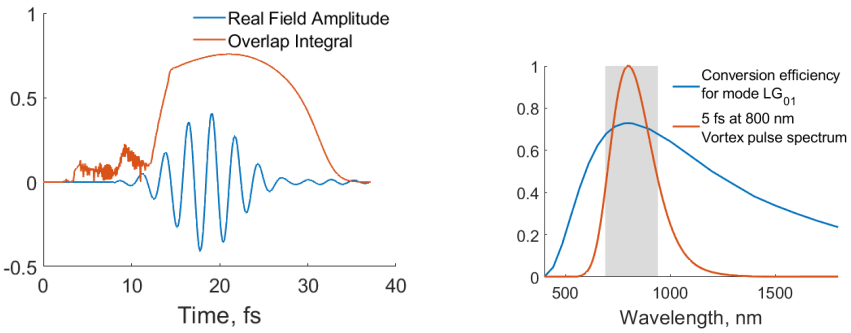

(a) (b)

Fig. 5: (a) Temporal real field amplitude and overlap integral between analytic LG_{01} mode (eq. 1) and generated ultrashort vortex pulse. (b) Conversion efficiency dependence in wavelength for an 8-levels SPP and spectrum of a $5fs$ vortex pulse at $\lambda = 800nm$.

is negligible on the temporal profile of optical vortex pulses (very small broadening at the studied temporal and spectral range), while the spatial profile and spatio-spectral properties of the vortex remained unchanged.

The analyzed SPP presents a conversion efficiency of more than 0.6 in a bandwidth from $630nm$ to $1050nm$. The results obtained in modeling vortex pulses can serve as a basis for novel devices design.

Acknowledgments. This work is supported by CONACyT via the PhD scholarship grant 763343 and by University of Guanajuato under research grant CIIC 272.2021.

References

1. Allen, L., Beijersbergen, M., Spreeuw, R.J.C.: Orbital angular momentum of light and transformation of Laguerre Gaussian Laser modes. Physical Review A 45(11), 8185–8189 (1992)
2. Beijersbergen, M., Coerwinkel, R., Kristensen, M., Woerdman, J.: Helical-wavefront laser beams produced with a spiral phaseplate. Optics Communications 112, 321–327 (1994)
3. Bozinovic, N., Yue, Y., Rena, Y., Tur, M., Kristensen, P., Huang, H., Willner, A.E., Ramachandran, S.: Terabit-Scale Orbital Angular Momentum Mode Division Multiplexing in Fibers. Science 340(6140), 1545–1548 (2013)
4. Foo, G., Palacios, D.M., Swartzlander, G.A.: Optical vortex coronagraph. Optics Letters 30(24), 3308–3310 (2005)
5. Malitson, I.H.: Interspecimen comparison of the refractive index of fused silica∗,†. J. Opt. Soc. Am. 55(10), 1205–1209 (Oct 1965), http://www.osapublishing.org/abstract.cfm?URI=josa-55-10-1205

6. Paterson, L., MacDonald, M.P., Arlt, J., Sibbett, W., Bryant, P.E., Dholakia, K.: Controlled Rotation of Optically Trapped Microscopic Particles. Science 292(5518) (2001)
7. Tamburini, F., Anzolin, G., Umbriaco, G., Bianchini, A., Barbieri, C.: Overcoming the Rayleigh Criterion Limit with Optical Vortices. Phys. Rev. Lett. 97(16) (2006)
8. Toda, Y., Nagaoka, K., Shimatake, K., Morita, R.: Generation and Spatiotemporal Evolution of Optical Vortices in Femtosecond Laser Pulses. Electrical Engineering in Japan 167(4), 39–46 (2009)
9. Wang, X.L., Luo, Y.H., Huang, H.L., Chen, M.C., Su, Z.E., Liu, C., Chen, C., Li, W., Fang, Y.Q., Jiang, X., Zhang, J., Li, L., Liu, N.L., Lu, C.Y., Pan, J.W.: 18-Qubit Entanglement with Six Photons' Three Degrees of Freedom. Phys. Review Letters 120(26) (2018)

Electronic edition
Available online: http://www.rcs.cic.ipn.mx

http://rcs.cic.ipn.mx

Centro de Investigación
en Computación